15

Bias current intrinsic field of the Hall sensor and its investigation unit

© H.R. Rostami, L.A. Lukanina

Fryazino Branch, Kotel'nikov Institute of Radio Engineering and Electronics, Russian Academy of Sciences,
141190 Fryazino, Moscow region, Russia
e-mail: rostami@ms.ire.rssi.ru

Received July 24, 2025
Revised December 9, 2025
Accepted December 17, 2025

The present study investigates influence of the intrinsic field of bias current through the Hall sensor on objects under study and accuracy of measurements of the Hall magnetometer. We have considered the intrinsic field of a heteroepitaxial sensor with a n-InSb$-i$-GaAs structure. For the studies, the unit is designed to move the studied sensor in relation to a measurement along the Z axis as far as 25 mm with accuracy $\sim 1\,\mu$m, to rotate the studied sensor around its axis for 360° with accuracy 2° as well as to linearly move it along the X axis as far as 5 mm with accuracy $\sim 1\,\mu$m. It is found that due to discontinuities of a circuit of power lines of intrinsic field induction edges of a thin epitaxial n-InSb film produce induction surges near Hall contacts of the sensor. With heterogeneous distribution of the bias current across a film cross section due to anisotropy and defects created by mechanical stresses in the film during its growth on a substrate, non-equipotentiality of the Hall contacts and with arbitrary arrangement of output sensor wires, it results in Hall contacts voltage that is superimposed onto a useful Hall signal, thereby causing an error.

Keywords: Hall sensor, Hall magnetometer, intrinsic field, bias current.

DOI: 10.61011/TP.2026.04.63279.195-25

Introduction

Up to now, in order to study magnetic and crystalline microstructures of physical, chemical, biological and other substances with high space and field resolution and within a wide range of magnetic and temperature field, 3D-scanning probe microscopes with the Hall effect sensors have been designed. For this purpose, the Hall probe scanners mainly use „cross" Hall sensors (HS) based on metal gold films and wires [1,2], semi-metal graphene and bismuth films [3–6], semiconductor thin epitaxial films based on silicon [7], high-performance InSb Hall microsensors for operation in wide ranges of the magnetic and temperature fields, GaAs-AlGaAs sensors with a two-dimensional electron gas [8].In connection with set tasks and specific features of their production technology, the above-listed Hall sensors differ by sizes of a working surface, sensitivity, bias current values, frequency, magnetic and temperature ranges of operation, etc.High spatial resolution is achieved by significantly reducing an area of the HS working surface. In order to ensure micro-displacement, the Hall sensor is fixed to a head of a piezoelectric scanner. In the studies [9–12], the high-performance In Hall microsensors were fabricated by photolithography and built in a scanning probe Hall microscope for studying spatial distribution of a captured magnetic flux (CMF) density and demagnetization fields on the surface of and around samples made of high-temperature superconductors (HTSC) [12] as well as for obtaining images of localized magnetic fluctuations in direct proximity to surfaces of uniaxial garnet crystal films at the room temperature [10]. Sensitivity of the InSb sensors is $(2.5-10)\cdot 10^{-7}$ T, which is by more than an order higher than that of the GaAs-AlGaAs sensors with the two-dimensional electron gas, which are used today [8]. However, as it is clear from these studies, simultaneous provision of high sensitivity and spatial resolution requires a compromise solution, since an increase of sensitivity results in reduction of spatial resolution and vice versa. Besides, unlike [9–12] the Hall sensors mentioned in [1–8] can provide high magneto-spatial resolution only in narrow ranges of the magnetic and temperature fields and do not make it possible to probe object surfaces at large spatial scales. Although in some of the listed studies authors notice a problem of influence of the intrinsic field of HS power current on the objects under study, this problem was still unstudied in detail. In turn, this did not make it possible to estimate a degree of influence of the intrinsic field H_{HT} of the bias current I_{HT} through the HS on sensitivity, linearity and accuracy of the Hall probe. In order to reduce influence of the field H_{HT} on the Hall probe parameters, the value of I_{HT} through the HC had to be reduced, thereby unavoidably resulting in drop of sensitivity and accuracy. In order to eliminate the above-listed disadvantages of the typical Hall probes, the studies [13,14] have demonstrated an operating principle of the two-stage Hall magnetometer of sensitivity $\sim 8\cdot 10^{-11}$ T with spatial resolution ~ 300 nm, which had a high degree of linearity and accuracy within the range of the magnetic fields $(10^{-11}-10^{-7})$ T. A hybrid Hall sensor based on a semiconductor n-InSb$-i$-GaAs Hall sensor and a thin HTSC twin epitaxial film $YBa_2Cu_3O_{7-x}$ (YBCO) was used as a sensitive zone. Unlike the classic magnetometers, an increase of spatial resolution in the proposed magnetometer results in not reduction, but, oppositely, an increase of sensitivity of the magnetometer, since local weak magnetic

field are recorded inside the HS working surface by means of individual „isolated“ uniformly-magnetized twins, whose magnetization increases with reduction of their sizes due to a significant increase of their critical currents. Thanks to a mechanism of field adjustment of the twin sizes of the YBCO HTSC film, spatial resolution of the probe can be changed within a wide range from the minimum twin size 10−20 nm to the size of the working surface of the first-stage Hall sensor $50 \times 100\,\mu$m. The first layer is also designed for simultaneous integral amplification of local fields of the uniformly-magnetized twins of the YBCO HTSC film. Consequently, the increase of the working surface of the Hall sensor results in an increase of its performance, while an increase of I_{HT} results in an increase of sensitivity of the Hall sensor (see below). In the studies [13,14], a basic first-stage magnetometer was the classic magnetometer designed to operate on the usual Hall effect with the PKhE 603 118 A, B Hall sensor and to provide sensitivity $\sim 2.5 \cdot 10^{-7}$ T within the dynamic range $(10^{-7} \pm 1.2 \cdot 10^{-1})$ T. The present study describes methods of investigating spatial distribution of the field H_{HT} and methods of increasing sensitivity both of an autonomous Hall sensor as well as the Hall sensor as the first stage of the hybrid two-stage magnetometer [13,14]. It will make it possible to find the degree of influence of H_{HT} on objects under study, sensitivity of the magnetometer as well as to contribute to designing methods of compensation of H_{HT}.

1. Discussion of the problem of origination of the intrinsic magnetic field near the Hall sensor and its influence on the parameters of the objects under study

It is found [7,15] that for the ideal Hall sensor (a symmetrical design, a homogeneous material, absence of side effects, etc.) when transmitting the bias current I_{HT} through the current contacts centrally applied to small butt-ends of a thin rectangular plate made of a high-resistance semiconductor material (of the width a, of the length ℓ and the thickness d) the Hall voltage V_{HH} originates in a magnetic field with induction $B_\perp$ perpendicular to the plate surface, on the transverse Hall contacts that are centrally arranged on the sides.

Fig. 1, *a* shows the schematic diagram of the Hall sensor. It is known [{]7,15} that

$$V_{\mathrm{HH}} = R_{\mathrm{HT}} B_\perp I_{\mathrm{HT}}/d, \qquad (1)$$

where R_{HT} is a Hall coefficient (in the weak magnetic field it does not depend on $B_\perp$ and is determined only by a semiconductor property). In the semiconductor plate with prevalent electron concentration $R_{\mathrm{HT}} = (e \cdot n)^{-1}$, where n and e are a concentration and the electron charge, respectively. Magnetic sensitivity of the Hall sensor is

$$\gamma = |V_{\mathrm{HH}}|(B_\perp)^{-1} = |R_{\mathrm{HT}}| I_{\mathrm{HT}} d^{-1} = I_{\mathrm{HT}}(end)^{-1} = [Pa\mu_e(d\ell en)^{-1}]^{1/2}, \qquad (2)$$

where P is power scattered on the Hall sensor, μ_e is mobility of electrons. As can be seen from the formula (2), for wide, short and thin HS working surfaces the higher mobility and the smaller the electron concentration, the higher HS magnetic sensitivity γ. According to multiple reference data, the high μ_e and the least n among all known semiconductors belong to the Hall sensors based on indium antimonide, which at the same time demonstrate more stable characteristics within the wide range of the temperature and magnetic fields. The current I_{HT} of the ideal Hall sensor with the wide and thin working surface can be mentally imagined as a summed current through parallel current threads with diameters that are equal to a film thickness. $I_{\mathrm{HT}} = \Sigma I_{\mathrm{HTi}}$. The currents I_{HTi} create solenoidal or vorticial fields B_{HTi}, whereas the fields between the threads compensate each other and as a result $B_{\mathrm{HT}} = \Sigma B_{\mathrm{HTi}}$ at both sides of the HS working surface are homogeneous and equal to each other.

Fig. 1, *b* shows distribution of power lines of induction BHT of the field H_{HT} around the HS current band. As seen from Fig. 1, *b*, the power lines of induction B_{HT} of the field H_{HT} form a circuit around the HS current band. Differently-directed power lines of induction B_{HT} are perpendicular to the HS current and parallel to the HS surface at both the sides: $B_{\mathrm{HT3}} = B_{\mathrm{HT}}(-a/2, 0, -d/2)$ and $B_{\mathrm{HT4}} = B_{\mathrm{HT}}(a/2, 0, d/2)$. At the same time, due to a

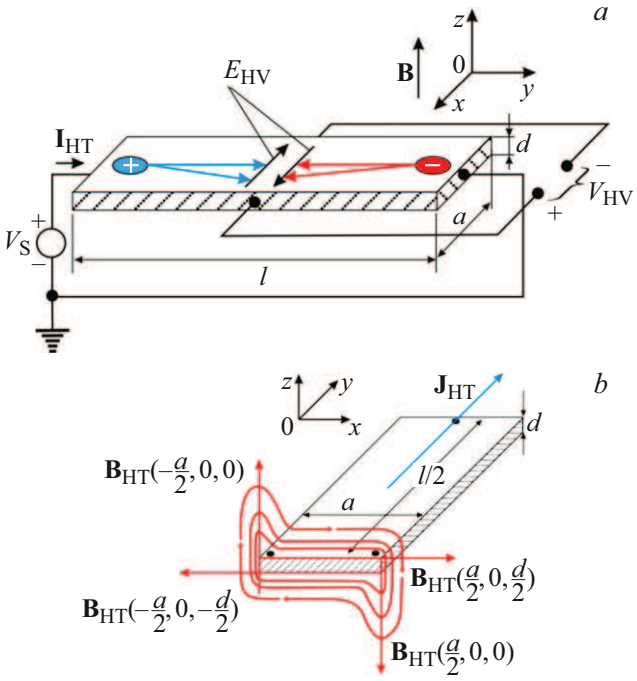

Figure 1. *a* — a schematic diagram of the Hall sensor; *b* — distribution of power lines of induction B_{HT} of the field H_{HT} around an HS current band.

significantly smaller film thickness as compared to its width the power lines at the edges get discontinuities that cause surges $B_{HT1} = B_{HT}(-a/2, 0, 0)$, $B_{HT2} = B_{HT}(a/2, 0, 0)$. In the real Hall sensors, values of these surges differ due to technological problems of production of the symmetrical Hall contacts, formation of nonuniformities, anisotropy of the film material, origination of defects due to mechanical stresses during growth on a film substrate, etc.It causes an unequal shift of the current and equipotential lines near the Hall contacts, thereby resulting in different magneto-concentration of the power lines of induction BHT and, consequently, the field BHT that is integral over an area of the sensitive element is non-zero. Thus, on the Hall contacts in the zero external magnetic field, in addition to origination of residual non-equipotentiality voltage and voltages caused by the Hall coefficient temperature dependences, induction BHT that is average over the area of the sensitive element and created by the differently-directed heterogeneous asymmetrical intrinsic field H_{HT} also generates additional voltage

$$V_{HT} \sim R_{HT} B_{HT} I_{HT}/d \sim R_{HT} I_{HT}^2/d. \quad (3)$$

In case of alternating current through the Hall sensor — $I_{HT} = I_0 \cos \omega t$,

$$V_{HT} \sim (R_{HT}/d) I_0^2 \cos^2 \omega t. \quad (4)$$

As seen from the formulas (3) and (4), the value of V_{HT} does not depend on a direction of current I_{HT}. The value of B_{HT} can be determined using a theorem of circulation of the vector **B**:

$$\oint \mathbf{B}\, d\,\mathbf{I} = \mu_0 I. \quad (5)$$

For points near the film surface and away from its edges

$$B = \mu_0 i/2 = (\mu_0 I)/2a, \quad (6)$$

where i is a current's linear density that is a current per a unit length of the film cross section. According to the formula (6), the PKhE 603 118 A, B Hall sensor used in the present study has:

$$B_{|textHT} = \mu_0 i_{HT}/2 = (\mu_0 I_{HT})/2a \approx 10^{-4} T. \quad (7)$$

2. Schematic diagram of the magnetometer and the magnetic field sensor chamber

Fig. 2, *a* shows the schematic diagram of the external controlling part of an insert of the magnetic field sensor chamber, which includes a mechanism of vertical movement of the studied HS2 along the Z axis in relation to a surface of the measuring HS1; a mechanism of rotation of HS2 around its axis within the XY plane and a mechanism of controlling a table of HS2 horizontal movement along the X axis.

Fig. 2, *b* shows the lower part of the insert of the magnetic field sensor chamber, which includes a copper disk with HS2 fixed on a head of the table for movement along the X axis; a copper disk with HS1, which is screwed in a brass guide rigidly fixed on an end of a central bar; a heater; a system of wiring to the HS, the heater and a thermometer. The system is operated in the following way: a micrometric screw is connected to a stainless steel rod via a system of a rotation-to-translation monitor converter and provides movement along the Z axis as far as 25 mm with accuracy $\sim 1\,\mu$m. In turn, via the system of the translation-to-rotation monitor converter the rod is connected to a flange by a thin-walled stainless tube that passes through brass guide sliders fixed on ends of the thin-walled stainless tube. The table of X movement is externally controlled via a worm gear by means of stainless steel rod that passes through the brass guide sliders fixed of the flanges of the rotating thin-walled stainless tube. Thus, the system provides independent control of the table. The disks have central cavities for installing HS1 and HS2, which are equal in height to their thickness and a diameter of the cavities corresponds to HS diagonals. The disk with the main measuring HS1 is fixed to an immobile bearing part of the insert, while the second disk with the studied HS2 is installed in the center of an X movement coordinate table. Measuring wires pass between coaxial thin stainless tubes of the central bar. A minimum distance between strictly parallel thoroughly polished surfaces of the copper disks, which comprise HS1 and HS2, is set by means of the film of the thickness $\sim 10\,\mu$m. For this purpose, the copper disk with HS2 is by means of a microscrew drawn nearer to the copper disk with HS1 along the Z axis until origination of an ohmic contact, which is followed by reversely shifting the copper disk with HS2 from a threshold of ohmmeter recording of ohmic contact break by $10\,\mu$m [16]. After specifying set values of Z and X the HS2 position is fixed in a horizontal plane. Further on, HS2 is rotated in relation to HS1 from $\varphi = 0$ to 360° with a step of 10° and for each φ values of B_{HT1} and B_{HT2} are measured. At the same time, in case of $X = 0$ a rotation axis passes through geometrical centers of HS1 and HS2. After movement of HS2 along the axes X or Z the measurements are again repeated while rotating HS2 in order to achieve maximum values of B_{HT1} and B_{HT2}. To compensate plays of threads of the microscrews, a start and an end of movement of HS2 along the axes X, Z and by the angle φ are controlled by means of ohmic contacts [16].

3. Operating principle of the magnetometer

In order to provide higher sensitivity, linearity, a high degree of accuracy, stability, a smaller temperature drift in time both for the HS and the magnetometer as well as the microscope based thereon within the wide range of the temperature and magnetic fields and frequencies, it is necessary to thoroughly compensate: residual bias voltage on the HS Hall contacts, which results without the external magnetic field due to non-equipotentiality of the Hall contacts; nonuniformity of distribution of physical parameters

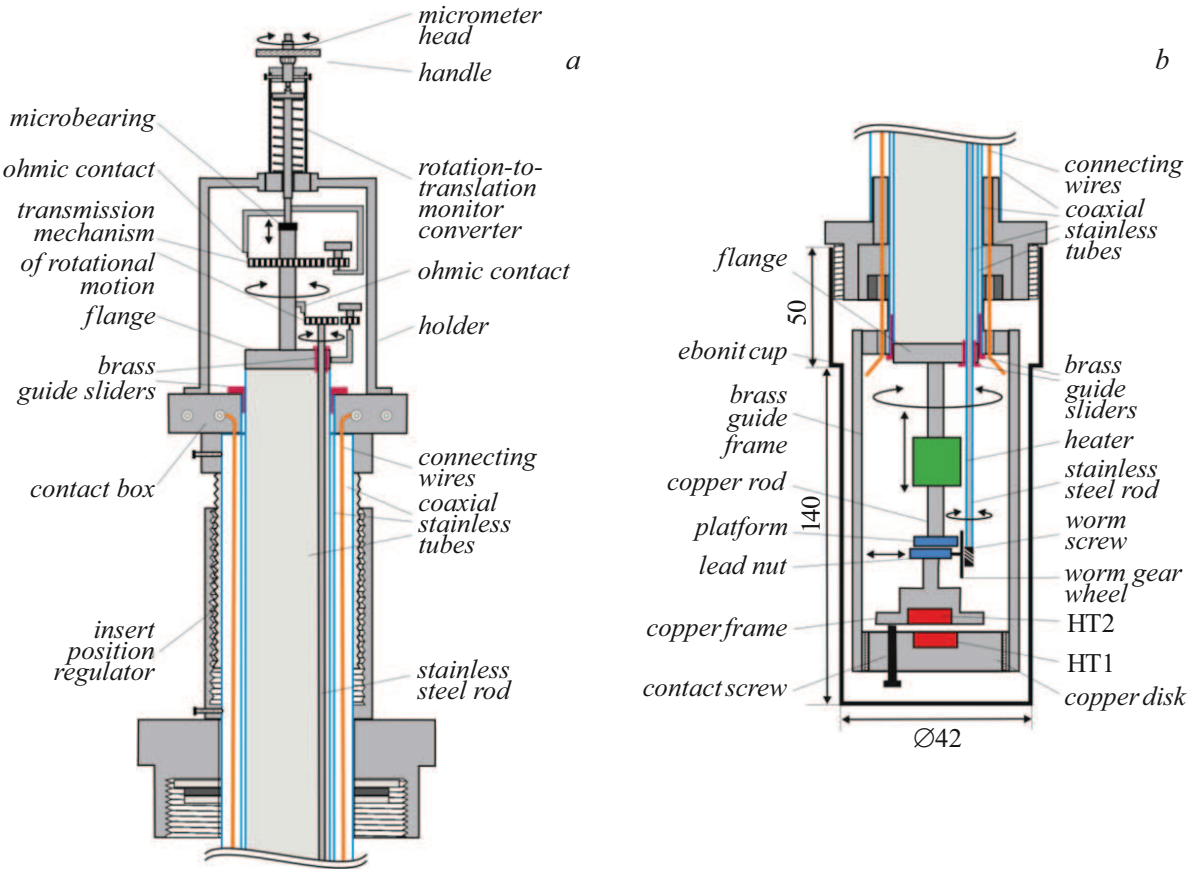

Figure 2. Schematic diagram of the magnetometer and the magnetic field sensor chamber: *a* — the external controlling part of the magnetic field sensor chamber; *b* — the lower part of the magnetic field sensor chamber.

of the HS film material; a piezoresistance effect caused by mechanical and temperature stresses of materials of the film and the substrate of the HS, which originate during a technological process of HS fabrication; systematic errors caused by the Hall coefficient's temperature dependence and other side effects. This compensation can be achieved when the HS is powered by a highly-stable alternating current with small nonlinear distortions and during HS operation in an isothermal mode. By averaging, it is possible to significantly compensate residual voltage, side effects caused by the Hall coefficient's temperature dependence, the field H_{HT}, the temperature drift of HS readings and a zero of an electronic part of microscope in time (see [16] and references cited).

Fig. 3 shows a block diagram of the magnetometer. The magnetometer is operated in the following manner: sinusoidal voltage that is highly-stable in terms of frequency and amplitude and has small nonlinear distortions is supplied from a sine-wave oscillator (SWO) to a precision current source (CS-1) with higher current stability. Alternating current $I_{\mathrm{HP}} = I_0 \cos \omega t$ passes from a source output through HS1 and produces voltage on the Hall contacts

$$V = V_{\mathrm{HH}} + V_{resid} + V_{\mathrm{HT}} + \Sigma V_i. \qquad (8)$$

In this expression V_{HH} is a useful Hall signal; V_{resid} — residual voltage of non-equipotentiality, which originates at the HS1 Hall contacts at the zero external magnetic field; V_{HT} — additional voltage originated in the intrinsic field H_{HT}; ΣV_i is total voltage of systematic errors (thermomagnetic voltage caused by the temperature effects and the Hall coefficient's temperature dependence). In order to record voltage V, the signals are supplied from the Hall contacts through voltage repeaters with high input resistances (that exclude influence of fields created by through input measuring currents of the repeaters) to inputs of a differential amplifier (DU) 1, whose output is connected to one of DU2 inputs, while the second input thereof is energized through a phase shifter 1 and a precision resistor R_1 from reference resistance R_{ref} connected in series to HS1, with voltage that is proportional to current I_{HT} through HS1. The DU2 output signal is supplied via a Π-shaped filter to the SD1 input, whose reference input is provided with a signal from SWO. Further on, the signal from the SD1 output is supplied to one of the DU3 inputs, whose second input is energized via the phase shifter 2 and the precision resistor R_2 from R_{ref} with voltage proportional to current I_{HT}. The output DU3 signal is supplied to the SD2 input, whose reference input is provided with a signal from SWO. This diagram solution provides a magnetometer output signal $V_{out} = K_u V_{in} \sim 10^5 V_{in}$. Thus, in the isothermal mode without the external magnetic field the proposed

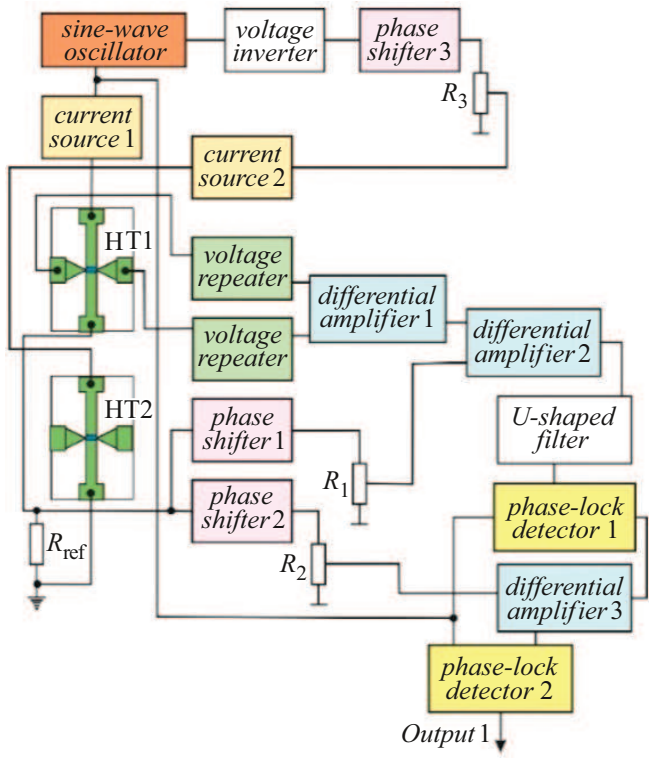

Figure 3. Block diagram of the magnetometer.

scheme makes it possible to compensate total voltage of errors $V_{resid} + V_{\text{HT}} + \Sigma V_i$approximately in $3 \cdot 10^5$ times and to amplify the useful signal V_{HH} in the same times when switching on the external magnetic field. A minimum level of the magnetometer's output signal is mainly determined by a threshold of HS1 magnetic sensitivity, which depends on characteristics of a semiconductor that is the material of the HS1 film. Depending on the level of the magnetometer input signal V_{in}, amplification coefficients of DU1-3 are specified irrespective of each other manually or by means of a computer. It makes it possible to provide an operating mode of DU1-3, which excludes a risk of their arrival into a saturation range. We not that the input and output resistances of the current sources CS1 and CS2 $R_{in} > 10^7\,\Omega$, $R_{out} > 10^8\,\Omega$, respectively. At the frequency of 1 kHz when $I_{\text{HT}} = 100\,\text{mA}$ and a load varied within $0-68\,\Omega$, current instability was below 0.005 %. A nonlinear harmonics coefficient within a band $0.1-1\,\text{kHz}$ is less than 0.01 %. Current instability for 8 h source operation at the frequency of 1 kHz with the load current of 100 mA at the room temperature $(20\,^\circ\text{C})$ was $< 0.01\,\%$. Among all the known semiconductors, n-InSb has the highest electron mobility adjusted within the range $\mu_e \approx (1.5-7.8)\,\text{m}^{-2}\text{V}^{-1}\text{s}^{-1}$, with the electron free path of $0.7\,\mu\text{m}$ at 300 K and electron concentration $(0.7-1.2) \cdot 10^{18}\,\text{cm}^{-3}$. The basic HS in the magnetometer was PKhE 603 118 A, B fabricated by photolithography based on the n-InSb$-i$-GaAs heteroepitaxial structure by growing a doped n-InSb epitaxial film of various sizes and a thickness on the single-crystal i-GaAs semi-insulating substrate (LLC „VEGA–FLEX", Saint-Petersburg) [9–12]. The PKhE 603 118 A, B with the external size of $3 \times 2 \times 0.6\,\text{mm}$ has the following parameters: the size of the working surface is $100 \times 50\,\mu\text{m}$; magnetic sensitivity is $0.81-1.28\,\text{V/T}$ when $B = 0.1\,\text{T}$ and the current is 100 mA; residual voltage is $30-60\,\mu\text{V}$; input resistance is $5.2\,\Omega$; output resistance is $7.5\,\Omega$; the operating temperature is $1.5-373\,\text{K}$; the temperature coefficient of magnetic sensitivity is $0.005\,\%/^\circ\text{C}$; the temperature coefficient of residual voltage is $0.2\,\mu\text{V}/^\circ\text{C}$. The nonlinearity coefficient is 0.3 % when $B = 2\,\text{T}$; the divergence coefficient is $< 0.1\,\%$ when $B = 0.1\,\text{T}$; the power current is 100 mA; the upper induction limit is 10 T. The Hall sensors with such characteristics provide linearity of 0.2 %–0.3 % within the field range up to 2 T, which significantly exceeds linearity of 2DEG AlSb/InAs sensors and other HS types. Besides, the n-InSb$-i$-GaAs Hall sensors have the highest specific sensitivity and relatively better metrological, field and temperature characteristics.

Since the signals from the Hall contacts and the reference resistance are leveled in an amplitude, any uncontrolled change of the amplitude of I_{HT} and its phase shift was additionally compensated by DU2. Without the external magnetic field, the magnetometer was adjusted by precision resistors R_1 and R_2 by alternately achieving the least reading of SD1 first and SD2 after that. Due to applying a procedure of initial subtraction–amplification–repeated twofold subtraction–amplification and using two-stage synchronous detection, error compensation accuracy is improved. It results in a significant increase of the level of $V_{\text{HH}}(B)$ as compared to a noise level, including intrinsic noise of operational amplifiers. In order to shield the Earth field and external interference, a cryostat was placed into a cylindrical magnetic screen that is made of an aluminum frame wrapped in a permalloy ribbon or a copper mesh and installed with its bottom on a permalloy disk fixed on a cryostat support. More precisely, the Earth magnetic field was compensated by means of a solenoid of inductance of $L_2 \approx 0.067\,\text{H}$, which was coaxial to a solenoid of inductance of $L_1 \approx 4.26\,\text{H}$, which created the external magnetic field. The insert of the magnetic field sensor chamber was placed inside coaxial to the solenoids. It was compensated by passing adjusted source direct current through the solenoid L_2. Thus, the proposed circuit diagram differs from traditional circuits of connection of the HS into a bridge arm and alternate pulsed switching of the current and Hall contacts at an integrator input, thereby causing pulsed interference that requires complicated circuits of their suppression.

4. Characteristics of the magnetic field sensor chamber and the magnetometer

Fig. 4 shows the block diagram of a microscope component for testing the following parameters: sensitivity;

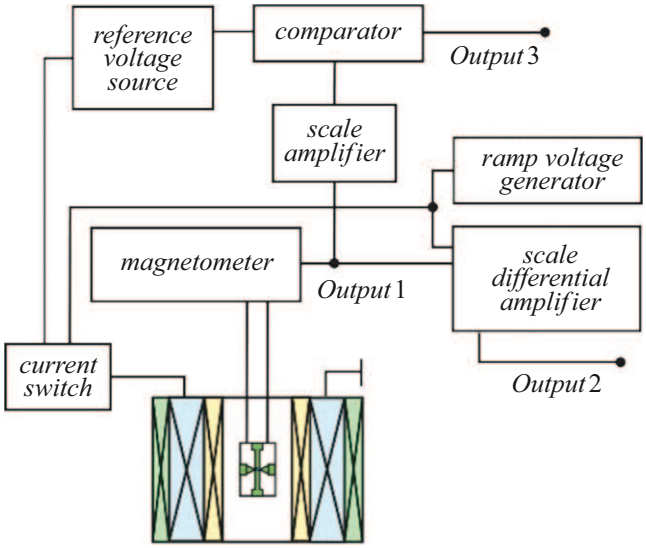

Figure 4. Block diagram of the component of the unit for testing parameters of sensitivity, linearity and accuracy for the magnetic field sensor chamber and the magnetometer.

linearity; accuracy of the output signal of the magnetic field sensor chamber and the magnetometer.

4.1. Magnetic sensitivity and methods of its determination

Magnetometer resolution was estimated by firstly finding a coil constant $K = H/I$ by means of the calibrated Hall sensor at a quite high current through the solenoid L_1. Then, for extremely small current through the solenoid L_1, with connecting the magnetometer output to one of comparator inputs, output voltage of the magnetometer was compared with voltage supplied to the second input of the comparator from an adjusted reference voltage source. Then, the current was passed through the solenoid and its value was adjusted until a surge at the comparator output. After that, the current value was determined and the formula $K = H/I$ was used to specify a minimum threshold of the field H, which makes it possible to calculate sensitivity of the magnetometer.

For clarity, Fig. 5, *a* shows the output signal of the comparator, wherein one of its inputs was provided with a reference signal proportional to the current through L_1 and the second one thereof was provided via the amplifier with the output signal of the magnetometer. While leveling the signals by adjusting the current through the solenoid, the output signal of the comparator surges from the state U_1 into the state U_2. It was found that sensitivity of the magnetometer without compensation of H_{HT} at the frequency of 19 Hz exceeds $2.5 \cdot 10^{-7}$ T. Although operation at the higher frequency 100–1000 Hz makes it possible to eliminate low-frequency interference (noise flicker $1/f$), but at such frequencies an essential role belongs to thermal noises (white noise, Johnson noises) of high resistance of the semiconductor as compared to the metal Hall sensors. Moreover, spurious capacitances greatly affect due to movement of moving microscope parts in space. With an increase of the operating frequency, a phase difference between V_{HH} and V_{resid} also increases, the shape of V_{HH} varies, thereby greatly affecting in case of recording of the weak magnetic fields. In order to reduced errors of measurements related to influence of the field H_{HT} on the HS readings and the physical parameters of the object under study, the field H_{HT} was thoroughly compensated. Compensation of the field H_{HT} was comparatively analyzed by three different methods: i — the measuring HS1 and the compensating HS2 were placed with front sides to each other; ii — HS2 was placed at a rear side of the HS1 substrate; iii — at the rear side of the HS1 substrate, on textolite of a printed circuit board we placed a copper bus that had the same geometrical sizes with HS1 and was produced by means of photolithography by etching a photoresist mask applied to the printed circuit board. After that, HS1 and HS2 or the copper bus were strictly parallel to each other placed into the cavity inside the immobile copper disk installed on the bearing lower part of the magnetic field sensor chamber (Section 1). Then, through HS2 or the copper bus we transmitted the current that was antiphase to the bias current I_{HT} through HS1. For this purpose, the signal from SWO was supplied through the phase shifter 3 and the precision resistor R_3 to the input of the precision current source CS2 that is identical to CS1 powering HS1. The CS2 output current was transmitted through a bifilarly wound (with a low wrapping pitch) wire to the HS1 supply wire, which was connected to HS2 or the copper bus. And adjusting the amplitude and the phase by means of the phase shifter and applying synchronous detection after each stage of compensation of the summed residual HS signal, we could improve sensitivity of the magnetometer from the level $\sim 2.5 \cdot 10^{-7}$ T to $\sim 5.3 \cdot 10^{-9}$ T in the case i (the curve *1* in Fig. 5, *a*); $\sim 5.75 \cdot 10^{-9}$ T in the case ii (the curve *2* in Fig. 5, *a*); $\sim 1.2 \cdot 10^{-8}$ T in the case iii (the curve *3* in Fig. 5, *a*).

4.2. Methods of determination of linearity and accuracy of the output signal of the magnetic field sensor chamber and the magnetometer based thereon

In order to determine the nonlinearity coefficient of the magnetometer a current that was linearly increasing in time was transmitted through the solenoid L_1 from the source and the output signals of the source and the magnetometer were compared.

Fig. 5, *b* shows time dependences of the output signal of the magnetometer, which is proportional to the current through the solenoid L_1 (the curve *1*), and the output signal of the source (the curve *2*) (Fig. 4).

Fig. 5, *c* a time dependence of the output signal of the differential amplifier, which is determined by a difference of

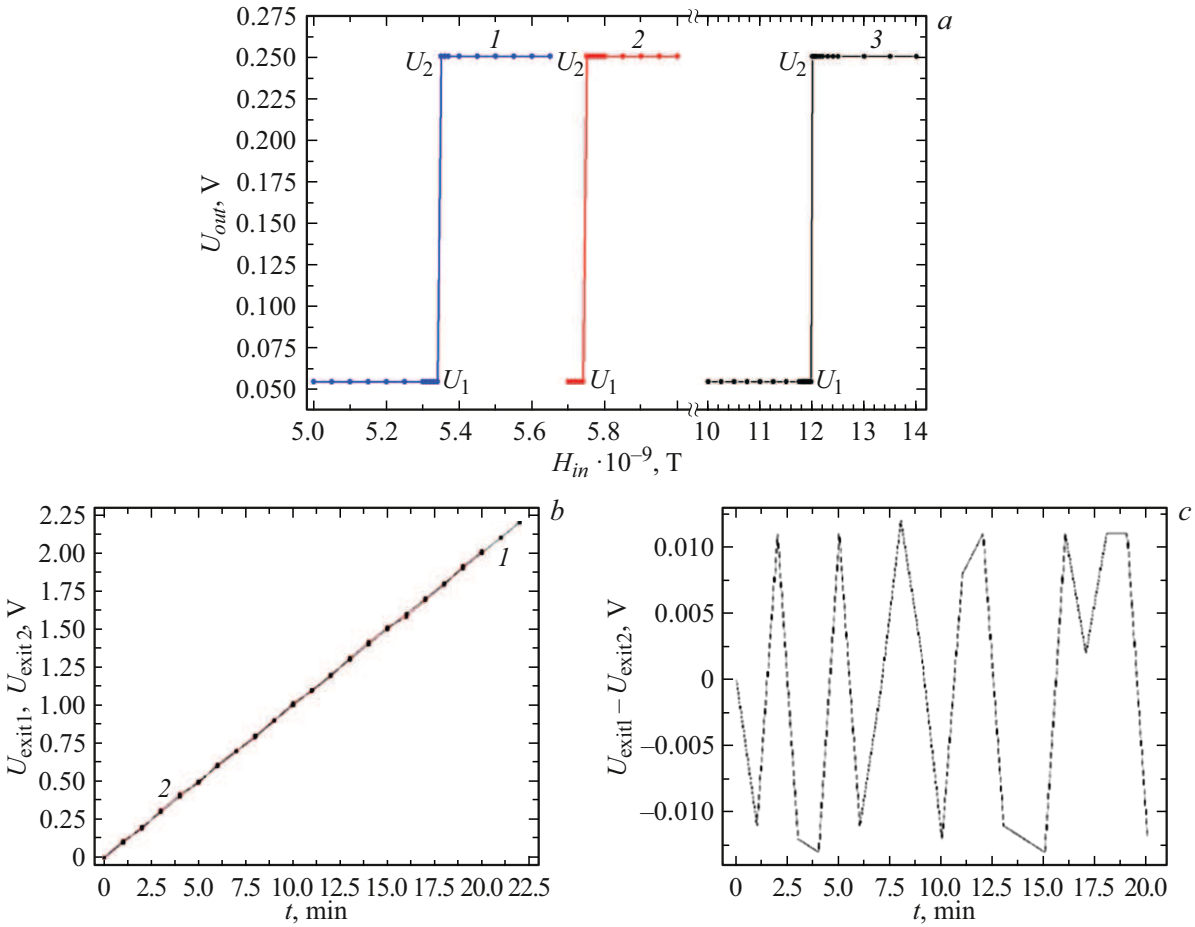

Figure 5. Output signal of the comparator, wherein one of its inputs was provided with a reference signal proportional to the current through L_1, and the second input was provided via the amplifier with the output signal of the magnetometer (a), the curves *1–3* correspond to a various geometry of the experiment (Section 4.1); time dependences of the output signal of the magnetometer, which is proportional to the current through the solenoid L_1 (the curve *1*), and of a sawtooth-voltage oscillator (the curve *2*) (b); time dependence of the output signal of the differential amplifier, which is determined by a difference of the output voltages of the magnetometer and the sawtooth-voltage oscillator (c).

the output voltages of the magnetometer and the source. According to a degree of deviation of the current and the field, as well as to the zero signal level at the differential amplifier, it was found that the nonlinearity coefficient of the magnetometer in the region of weak fields was $< 0.003\,\%$ and decreased with a signal level increasing. It should be noted that the nonlinearity coefficient of the magnetometer [12,16] with the uncompensated Hall sensor was $< 0.01\,\%$ and mainly specified by HS nonlinearity, which is below $0.04\,\%$ when $B = 2$ T. In the region of weak fields, the Hall sensor exhibits linearity that is higher (below $0.01\,\%$) than that specified in a data sheet. The temperature drifts of the HS parameters were reduced by specifying and constantly maintaining the temperature with instability below 0.01 K in the gas-flow microcryostat or the microscope's measuring part was placed in liquid nitrogen. According to the HS data sheet, the temperature coefficients were: V_{HH} below $0.08\,\mu$V/K and V_{resid} below $0.54\,\mu$V/K. Moreover, after each specified temperature disbalance signals caused by thermal effects were additionally compensated by means of an electronic circuit.

Thus, it is clear from the results obtained that the more accurate compensation of the field H_{HT}, it is easier to improve sensitivity of the magnetometer while preserving high linearity, accuracy, stability and repeatability of the measurement results when they are averaged for long time of operation of the magnetometer within a dynamic range of the fields $(0.1-5) \cdot 10^{-8}$ T and the temperatures 77.4–150 K.

It also follows from these comparisons that it is possible to increase the degree of linearity and accuracy of the magnetometer by more than an order when using the Hall sensors with the compensated field H_{HT} in the magnetometers [12,16]. Besides, in order to achieve high resolution, accuracy and linearity of the magnetometer within the entire range of measurements, it is necessary to discretely divide a range of recorded fields of the magnetometer by one's own strictly fixed parameters.

In order to determine the value and spatial distribution of the field H_{HT}, we have studied a drop of axial distribution $H_{\mathrm{HT}}(Z)$ during vertical movement of HS2 uncompensated by H_{HT} in relation to the surface of HS1 compensated by H_{HT}. Moreover, for detailed clarification of mechanisms of origination of H_{HT} in the real Hall sensors we have also comparatively analyzed results obtained by means of the Hall sensors that have various sizes of the working surfaces. The experiment was performed with HS1 and HS2 and sizes of their working surfaces were taken in various options: 50×00, 150×450, 250×1000, 500×1500, $500 \times 2000\,\mu$m [9]. At the same time, a direct or alternating current of the value of 100 mA was transmitted through HS1 and HS2.

5. Experimental techniques and samples

The studies were in modes FC (field cooling), ZFC (zero field cooling) [12,16]. The studies were performed on YBCO single crystals with $T_c \approx 91$ K, of the sizes $\sim 1 \times 1 \times 0.05$ mm (the sample No. 1); single crystals $Bi_2Sr_2CaCu_2O_{8+x}$ (BSCCO) with $T_c \approx 90.2$ K, of the sizes $\sim 4 \times 4 \times 0.1$ mm (the sample No. 2); bulk textured (the c axis is perpendicular to the sample plane) quasi-single-crystal (melt) YBCO samples No. 3, polycrystalline samples No. 4 textured along the c axis and non-textured ceramic YBCO HTSC samples No. 5; epitaxial YBCO films with the c axis that is perpendicular to the plane of the $NdGaO_3$ substrate(110) (the sample No. 6). The samples shaped as a disc of the diameter of $D \sim 6-8$ mm and the thickness of $h \sim 0.4-1.0\,\mu$m (films) and $\sim 0.7-4.3$ mm (bulk samples Nos. 3–5) had $T_c \approx 92$ K and a transition width $\Delta T_c \approx 0.6-1$ K.

The following experiments were performed in order to estimate a degree of compensation of voltage V_{HT} originating in the intrinsic field H_{HT}.

1. First, without compensation of H_{HT} the YBCO sample was moved towards HS1 in the ZFC mode along the Z axis and it was found that the disbalance signal was reduced at the magnetometer output. When the sample was taken away from HS1, the disbalance signal returned to its initial value, while drawing again the sample nearer to the HS1 surface resulted in the increase of the disbalance signal. Then, in the FC mode the YBCO HTSC sample nearer HS1 was heated to the temperature above T_c and cooled again to the liquid nitrogen temperature $T = 77.4$ K. This experiment exhibited an even greater increase of the disbalance signal at the magnetometer output as compared to the ZFC mode - when the sample in a superconducting state was drawn nearer to the HS1 surface. As in the first experiment, when the YBCO sample was taken away from the HS1 surface, the disbalance signal was decreasing to take on its initial value. In the ZFC mode, variation of the output signal of the magnetometer is caused by demagnetization fields of the YBCO samples, which are induced by the field H_{HT} [12]. In the FC mode, when the YBCO sample near the HS1 surface was cooled from the temperature above T_c to the temperature of 77.4 K, H_{HT} penetrated deep inside the sample through Josephson weak bonds. When the sample was taken away from the HS1 surface, the sample experienced magnetic flux capture (MFC) by the created field H_{HT}, which resulted in the increase of the disbalance signal at the magnetometer output when drawing the sample again nearer the converter. The similar results were also obtained when replacing the sample No. 1 with the samples Nos. 2–6. However, for the sample No. 2 due to the low first critical magnetic field H_{c1} and the higher MFC density $B_{tr}^{\max}(0)$ as compared to the sample No. 1 — the disbalance signal at the magnetometer output was increasing. For the samples Nos. 3–5 — due to the lower H_{c1} and the significantly high $B_{tr}^{\max}(0)$ as compared to the samples Nos. 1, 2, 6 — the disbalance signal at the magnetometer output was even more increasing. When a ferromagnetic film was drawn nearer to the HS1 surface, H_{HT} was significantly amplified (due to its high permeability), thereby resulting in the increase of the disbalance signal by more than an order. Therefore, in case of using magnetic concentrators with high permeability for amplifying and focusing power lines of magnetic field induction on the HS surface [17], it must be borne in mind that it will result in both amplification of magnetic sensitivity as well as degradation of HS spatial resolution.

2. For the modes FC and ZFC, when repeating the experiment with the compensated H_{HT}, we have found that in case of drawing both the superconducting film as well as the magnetic film nearer to the HS1 surface the output voltage of the magnetometer did not change.

6. Experimental results and their processing

In order to find the value and spatial distribution of $B_{\mathrm{HT}}(\varphi, X, Z)$ on the surface of and around HS2, we have probed a topology of the field $B_{\mathrm{HT}}(\varphi, X, Z)$ by means of movement of the studied HS2 uncompensated for H_{HT} in relation to the surface of the measuring HS1 compensated for H_{HT}. In order to study distribution of the power lines of induction BHT of the field H_{HT} around the HS2 Hall contacts, first of all values of B_{HT} on one of the Hall contacts were measured, so was its variation along a line connecting this Hall contact with the Hall contact on an opposite HS2 facet along the X axis by means of the linear movement table. In this case, the line connecting the HS2 Hall contacts coincided with the line connecting the HS1 Hall contacts, i.e. at ends of these lines the angles were $\varphi_1 = 0^\circ$ and $\varphi_2 = 180^\circ$. Then, by alternately changing the coordinates X, Z and by rotating HS2 for the angle φ around its axis that coincides with the axis passing through a HS1 geometrical center, distribution of B_{HT} on the HS2 surface was mapped by means HS1. It should be noted that with an increase of Z SP1 covers an ever larger area of the SP2 working surfaces and makes it possible to observe not only distribution of the power lines of B_{HT1} and B_{HT2} near both the Hall contacts, but distribution of their summed field

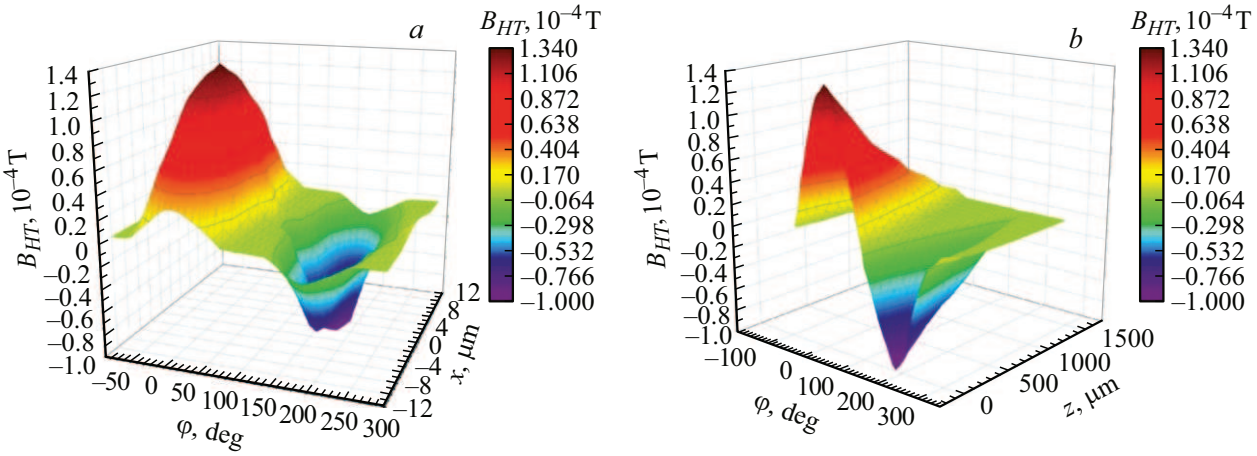

Figure 6. 3*D*-dependences $B_{\mathrm{HT}}(\varphi, X, Z)$ in cases when at the specified Z φ and X vary (a); at the specified X φ and Z vary (b).

on the HS2 surface and enables tracing dynamics of their change in a dependence on φ, X, Z. It makes it possible to ascertain zeroing of the total signal at the HS1 output and, respectively, the output voltage of the magnetometer when leveling the values of B_{HT1} and B_{HT2}.

Fig. 6 shows 3*D*-dependences $[B_{\mathrm{HT}}(\varphi, X, Z)](\varphi, X, Z)$ in cases when at the specified Z φ and X vary (Fig. 6, *a*); at the specified X φ and Z vary (Fig. 6, *b*). Ranges and patterns of the increase and drop are clearly visible in Fig. 6. $B_{\mathrm{HT}}(\varphi, X, Z)$.

Thus, as seen from the given studies, the topology of distribution of the field H_{HT} over the surface of and around the HS is highly heterogeneous. Therefore, it must be borne in mind that interaction of the field H_{HT} with local fields on the surface of the samples when they are mapped will result significant distortion of three-dimensional distribution, for example, of such magnitudes as the MFC density on the surface of the HTSC samples and magnetization of magnetic materials. Usually, in order to improve spatial resolution of the magnetometer, one has to place the Hall sensors too close to the surface of the object under study. However, as seen from Fig. 6, *b*, for the above-said Hall sensors the dependence $[B_{\mathrm{HT}}(\varphi, X, Z)/B_{\mathrm{HT}}(0)^{\max}](Z)$ reaches zero during approximation when $Z \geq 2$ mm. Therefore, in order to improve spatial resolution of the magnetometer, it is necessary to preliminarily compensate the field H_{HT} of the used Hall sensor, thereby making it possible to place the Hall sensor much closer to the surface of the object under study, without affecting the local fields distributed over its surface. Usually, in order to improve spatial resolution, one has to reduce a size of the area of the HS working surface, while reduction of the field H_{HT} requires reduction of the value of the current I_{HT}. In this respect, it must be borne in mind that in addition to sensitivity loss, poor heat removal the high temperature drift of the HS readings in time, which results in low stability of operation of such Hall sensors, the ratio $H_{\mathrm{HT}}/I_{\mathrm{HT}}$ will be of the same order with this ratio for the HS with high I_{HT} and H_{HT}. So for closer approximation of any HS to the surface of the object under study and improvement of HS sensitivity, the field H_{HT} must be compensated first.

As known [9–12], the thickness of the i-GaAs substrate for the PKhE 603 118 A, B Hall sensors and other Hall sensors of this series is $\sim 600\,\mu$m; on the other hand, Fig. 6, *b* demonstrates that when the HS surface is removed as far as $\sim 600\,\mu$m B_{HT} drops approximately by 40 %. Hence, comprehensive compensation of B_{HT} requires to increase an amplitude of antiphase current through the copper compensating band approximately by 40 % as compared to the current I_{HT} through the HS. Moreover, due to loose parallelism of the main and compensating current buses and a distance $\sim 600\,\mu$m therebetween, it is necessary to adjust not only the amplitude, but a phase of the current through the copper compensating bus. According to [13,14], in order to improve spatial resolution of the magnetometer when measuring distribution of the MFC density inside the twins that have small sizes up to 10–25 nm and at a twinning boundary, it is necessary to measure the local fields inside the HS working surface. Besides, for significant amplification of the local fields, it is necessary to use the Hall sensor with large sizes of the working surfaces and with the high current I_{HT}. It should be noted that it will result in an increase of the field H_{HT} as compared to the Hall sensor powered by small currents I_{HT} and made with smaller sizes. Nevertheless, due to a high amplification coefficient of Hall voltage, high spatial resolution and stabler operation, it is preferable to use the Hall sensor of large sizes with the high currents I_{HT} [13,14].

Conclusion

It is found that with removal from the HS surface as far as $\sim 600\,\mu$m normalized axial distribution $[B_{\mathrm{HT}}(\varphi, X, Z)/B_{\mathrm{HT}}(0)^{\max}](Z)$ drops by ~ 40 %. Since the thickness of the i-GaAs substrate for the PKhE 603 118 A, B Hall sensor is $\sim 600\,\mu$m, for comprehensive compensation of B_{HT} and operational reduction of the errors, it is

necessary to increase the amplitude of the antiphase current through the compensating band by $\sim 40\,\%$ as compared to the current I_{HT} through the measuring HS. Moreover, due to loose parallelism of the measuring and compensating current buses and the distance $\sim 600\,\mu$m therebetween, it is necessary to adjust not only the amplitude, but the phase of the compensating current through HS2 and the copper bus that is parallel to the HS current band, thereby making it possible to improve sensitivity of the Hall magnetometer by more than an order.

It also follows from the obtained results that in order to achieve higher accuracy and to simplify a procedure of compensation of H_{HT}, it is necessary to grow the same (close in terms of technical parameters) thin epitaxial n-InSb films during HS fabrication at both sides of the single-crystal semi-insulating i-GaAs substrate in a unified process cycle.

When using this magnetometer as the first stage of the two-stage magnetometer described in [13,14], it is possible to increase its sensitivity to $\sim 10^{-12}-10^{-13}$ T while preserving the high degree of linearity, accuracy, stability and repeatability of the measurement results when they are averaged for long time of operation of the magnetometer.

Funding

This study was carried out under the state assignment of the Kotelnikov Institute of Radio Engineering and Electronics of the Russian Academy of Sciences.

Conflict of interest

The authors declare that they have no conflict of interest.

References

[1] M. Gerken, A. Solignac, D. Momeni Pakdehi, A. Manzin, T. Weimann, K. Pierz, S. Sievers, H.W. Schumacher. J. Sens. Sens. Syst., **9**, 391 (2020).
[2] A. Sandhu, A. Okamoto, I. Shibasaki, A. Oral. Microelectron. Eng., **73**–**74**, 524 (2004).
[3] G. Shaw, R.B.G. Kramer, N.M. Dempsey, K. Hasselbach. Rev. Sci. Instrum., **87**, 113702 (2016).
[4] M. Dede, R. Akram, A. Oral. Appl. Phys. Lett., **109**, 182407 (2016).
[5] P. Li, D. Collomb, Zh.J. Lim, S. Dale, Ph. Shepley, G. Burnell, S.J. Bending. Appl. Phys. Lett., **121**, 043502 (2022).
[6] D. Collomb, P. Li, S. Bending. J. Phys.: Condens. Matter, **33**, 243002 (2022).
[7] H.P. Baltes, R.S. Popović. IEEE, **74** (8), 1107-1 (1986).
[8] K. Vervaeke, E. Simoen, G. Borghs, V.V. Moshchalkov. Rev. Sci. Instrum., **80**, 074701 (2009).
[9] Electronic media. Available at: http://sensorspb.ru/price5.doc
[10] A.I. Rokeakh, M.Yu. Artyomov. Rev. Sci. Instrum., **94**, 034702 (2023).
[11] V.K. Ignat'ev, A.A. Orlov, S.V. Perchenko, D.A. Stankevich. Tech. Phys. Lett., **43** (15), 687 (2017).
[12] Kh.R. Rostami. Supercond. Sci. Technol., **36**, 095012 (2023).
[13] Kh.R. Rostami, I.P. Nikitin. Measurement, **153**, 107423 (2020).
[14] Kh.R. Rostami, I.P. Nikitin. Sensors and Actuators A: Physical., **346**, 11384 (2022).
[15] R.S. Muller, T.I. Kamins. *Device Electronics for Integrated Circuits* (John Wiley and Sons, Inc, 1977, 1986)
[16] Kh.R. Rostami. Tech. Phys., **65** (12), 1975 (2020).
[17] R.S. Popovic. *High Resolution Hall Magnetic Sensors*. PROC 29th Int. Conf. on Microeletronics (MIEL 2014) (Belgrad, Serbia, 12–14 May, 2014), p. 69–74.

Translated by M.Shevelev